

Solid lipid nanoparticles self-assembled from spray dried microparticles

Brenda Sanchez-Vazquez,^a Jong Bong Lee,^b Margarita Strimaite,^a Asma Buanz,^a Russell Bailey,^c Pavel Gershkovich,^b George Pasparakis^a and Gareth R. Williams^{a*}

^a UCL School of Pharmacy, University College London, 29-39 Brunswick Square, London WC1N 1AX, UK.

^b Centre for Biomolecular Sciences, University of Nottingham, University Park, Nottingham NG7 2RD, UK.

^c School of Engineering and Materials Science, Queen Mary University of London, Mile End Road, London, E1 4NS, UK.

* Corresponding authors. Email: g.pasparakis@ucl.ac.uk; g.williams@ucl.ac.uk

Abstract

We report the self-assembly of anti-cancer drug-loaded solid lipid nanoparticles (SLNs) from spray dried microparticles comprising poly(vinylpyrrolidone) (PVP) loaded with glyceryl tristearate (GTS) and either indomethacin (IMC) or 5-fluorouracil (5-FU). When the spray dried microparticles are added to water, the PVP matrix dissolves and the GTS and drug self-assemble into SLNs. The SLNs provide a non-toxic delivery platform for both hydrophobic (indomethacin) and hydrophilic (5-fluorouracil) drugs. They show extended release profiles over more than 24 h, and in permeation studies the drug cargo is seen to accumulate inside cancer cells. This overcomes major issues with achieving local intestinal delivery of these active ingredients, in that IMC permeates well and thus will enter the systemic circulation and potentially lead to side effects, while 5-FU remains in the lumen of the small intestine and will be secreted without having any therapeutic benefit. The SLN formulations are as effective as the pure drugs in terms of their ability to induce cell death.

Our approach represents a new and simple route to the fabrication of SLNs: by assembling these from spray-dried microparticles on demand, we can circumvent the low storage stability which plagues SLN formulations.

27 **Keywords**

28 Spray-drying; self-assembly; solid lipid nanoparticle; drug delivery system; stability

29

30 **1. Introduction**

31 Solid lipid nanoparticles (SLNs) are colloidal drug carriers of size between 50 – 400 nm which have
32 been much explored as an alternative to emulsions, liposomes, and polymeric particles. They contain
33 solid lipids such as fatty acids, steroids, glycerides and waxes in place of the liquid lipids which are
34 employed for other formulations (Muller et al., 1995). SLNs are advantageous over other lipid-based
35 systems in terms of their small size, large surface area, and high biocompatibility (owing to the low
36 toxicity of their components) (Mehnert and Mäder, 2001). In addition, they can provide highly
37 controlled drug delivery. There is thus great interest in the use of SLNs as drug nanocarriers
38 (Mukherjee et al., 2009), for instance in the improvement of treatments for various types of cancer
39 (Chen et al., 2001; Kang et al., 2010; Lee et al., 2007; Yang et al., 1999). However, there are a number
40 of drawbacks to SLNs, including a limited drug-loading capacity and sometimes rapid expulsion of the
41 encapsulated drug. A major problem is the commonly reported gelation of SLN dispersions, and a
42 marked increase of their particle size upon storage owing to poor colloidal stability (Das and
43 Chaudhury, 2011).

44

45 The most common processes for fabricating SLNs are high pressure homogenization or sonication
46 (Mehnert and Mäder, 2001, 2012). Both involve melting the lipid and drug, followed by the formation
47 of an emulsion by dispersing the melt into a hot aqueous surfactant solution. Subsequent cooling of
48 the emulsion allows the solidification of the lipid, giving an aqueous dispersion of SLNs. These
49 aqueous dispersions can then be converted into a dry powder to improve storage stability (Mehnert
50 and Mäder, 2001, 2012). This multi-step process is time consuming and expensive however, and the
51 use of heat can be problematic for thermally labile drugs. Alternative SLN manufacturing processes
52 are thus much sought after (Mehnert and Mäder, 2012).

53

54 One alternative approach to SLN fabrication involves the use of polymer-based microcomposites as
55 sacrificial templates. In this paradigm, a fast-dissolving hydrophilic matrix containing the drug and
56 lipid as a molecular dispersion is first prepared, and then added to water. As the hydrophilic matrix
57 takes up water, the hydrophobic components (the drug and lipid) cluster together and self-assemble
58 into SLNs. This route has been proven viable using polymer composites generated by
59 electrohydrodynamic (EHD) approaches, as reported by Yu *et al.* (Yu et al., 2011a). However, although
60 EHD approaches are increasingly recognised as being scalable from the lab bench to industrial
61 production volumes (Démuth et al., 2016; Farkas et al., 2019; Valtera et al., 2019; Vass et al., 2019),
62 the vast majority of research on them has to date been performed at small scale, and the techniques
63 have yet to be adopted by the pharmaceutical industry.

64

65 In contrast, the spray drying approach to preparing polymer-based composites is widely used in the
66 pharmaceutical (and food) industries for a variety of applications (Poozesh and Bilgili, 2019; Ziaee et
67 al., 2019). It involves rapid evaporation of the solvent from a solution, and results in spherical
68 particles of around 1 – 5 µm in size. Spray drying has extensively explored to generate formulations
69 of active pharmaceutical ingredients (APIs), with systems containing etravirine, ivacaftor, tacrolimus,
70 itraconazole, and everolimus, among many others, having been reported (Newman, 2015; Ziaee et
71 al., 2019). Typically spray dried microparticles comprise amorphous solid dispersions, offering
72 advantages in solubility and dissolution rate over other formulation approaches.

73

74 Spray drying has also been studied for developing SLN and other nanoparticulate-based formulations.
75 There are four different approaches that can be envisaged. In the first (Figure 1(a)), a suspension of
76 SLNs can be spray dried into a dry reconstitutable powder. This has been reported on a number of
77 occasions, but obstacles such as particle growth have been encountered as a consequence of the use
78 of high temperatures and the resultant melting of the lipid phase (Salminen et al., 2019). Extensive

79 optimisation is also required (Xia et al., 2016). The second method uses the spray-drying technique
80 for the top-down preparation of nanoparticle-loaded polymer microparticles, by processing
81 suspensions of nanoparticles in a polymer solution (see Figure 1(b)). The resultant formulations have
82 been found to have potential for the formulation of APIs for delivery by multiple administration
83 routes (Müller et al., 2000). Both these methods require the SLNs to be prepared prior to spray
84 drying, rendering them rather complex multi-step processes.

85

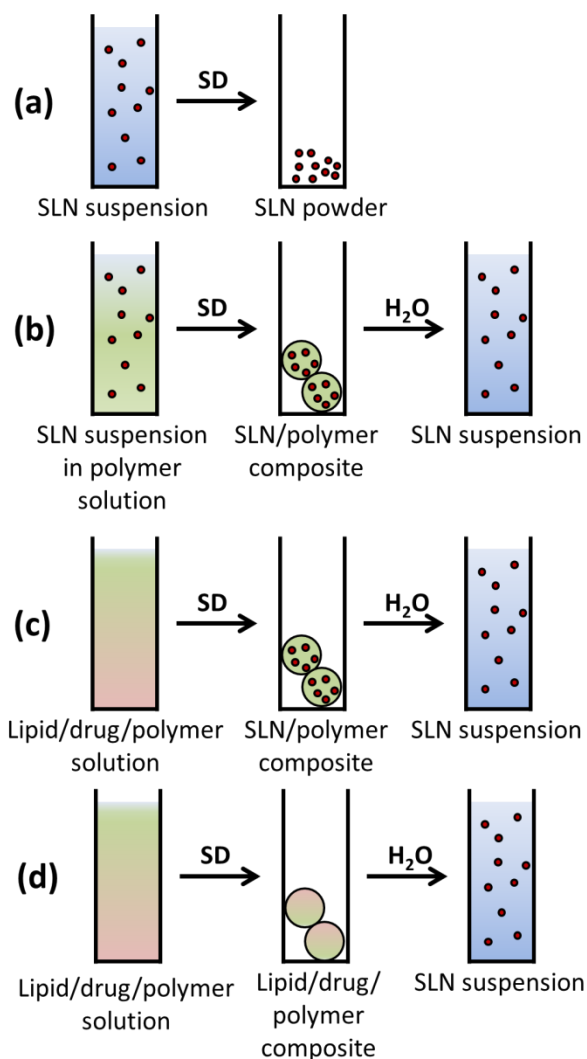
86 A potentially more interesting application of spray drying is its putative use in the bottom-up self-
87 assembly of nanoscale objects. In the case of SLNs, this would involve processing a solution of drug,
88 lipid, and polymer. These could either self-assemble into SLNs during the drying process (Figure 1(c)),
89 or produce a molecular dispersion of drug and lipid in polymer (Figure 1(d)). Such bottom-up self-
90 assembly is a much simpler route to nanoscale systems than the top-down method, and can be
91 completed in two steps (preparation of the microparticles, and then addition of the solvent). There
92 are several reports of the former in the literature. For instance, Pansare et al. have used this to self-
93 assemble nanocrystals of phenytoin in a hydroxypropyl methylcellulose / poly(lactic acid)-
94 poly(ethylene glycol) block copolymer by spray drying (Pansare et al., 2018), while Liu and co-workers
95 have generated core/shell microparticles with a Eudragit RS shell and silica sol core (Liu et al., 2011).
96 In both cases, complex architectures could be obtained in a single step during drying. In related work,
97 Suhendi et al. were able to assemble silica nanoparticles and polystyrene spheres during the spray
98 drying process (Suhendi et al., 2013), and Fatnassi combined sol-gel approaches with spray-drying to
99 obtain drug-loaded nanostructured microparticles (Fatnassi et al., 2010).

100

101 To date, to the best of our knowledge, there are no reports in the literature of the final situation, in
102 which a molecular dispersion is generated by spray drying and then self-assembles upon addition to
103 water. There are also no reports of self-assembling SLNs in spray drying, despite the great benefits
104 of these systems. In this work, we sought for the first time to self-assemble SLNs from spray dried

105 formulations. To do this, we employed the hydrophilic polymer poly(vinylpyrrolidone) (PVP), the solid
106 lipid glyceryl tristearate (GTS), and either 5-fluorouracil (5-FU) or indomethacin (IMC), two drugs with
107 potential in the treatment of colon cancer (Foley et al., 2008; Hull et al., 2003; Wang and DuBois,
108 2006). We hypothesised that the PVP-based microparticles produced could act as “proto-SLNs”,
109 allowing us to produce formulations which are long-term stable and can be converted to SLNs on
110 demand.

111



113

114 Figure 1: Schematic illustrations of the different approaches to produce drug-loaded SLN-based formulations by spray drying (SD). (a)
 115 A suspension of drug-loaded SLNs can be converted into a powder; (b) a suspension of drug-loaded SLNs in a polymer solution yields
 116 SLN/polymer composites, which can later dissolve to give free SLNs; (c) a solution of lipid, drug, and polymer can be converted into
 117 SLN-loaded polymer particles in the SD step, and again the latter can be dissolved in an aqueous medium to free the SLNs, and (d) a
 118 lipid/drug/polymer solution can be processed into a molecular dispersion composite, which then self-assembles into drug-loaded
 119 SLNs when water is added.

120

121 2. Materials and methods

122 2.1 Synthetic procedures

123 Solutions containing indomethacin (IMC, Alfa Aesar) or 5-fluorouracil (5-FU, Sigma-Aldrich) were prepared
 124 prior to the spray drying process. These solutions were composed of the drug, polyvinylpyrrolidone (PVP, 40

125 kDa, Sigma-Aldrich) and glyceryl tristearate (GTS, Sigma-Aldrich). Chloroform was used as the solvent for IMC.
126 In the case of 5-FU, the drug was fully dissolved in dimethylformamide (DMF) and then mixed with a PVP/GTS
127 solution in chloroform for 10 min before spray drying. All solvents were from Fisher Scientific. The solutions
128 contained final concentrations of 10 % w/v of polymer, 5 % w/v of GTS and 2.5 % w/v drug.

129
130 Spray drying was performed using a mini spray dryer (Buchi B-290, Laboratory-Technik Ltd) with a closed
131 loop. The spray nozzle tip diameter was 0.7 mm. The inlet air temperature was 70 °C and the outlet air
132 temperature 40–48 °C. The liquid feed rate to the dryer was 10 mL min⁻¹, and the flow of drying gas
133 approximately 35 m³ h⁻¹. Experiments were performed under constant process conditions. After letting the
134 equipment cool down to below 50 °C, the dry powder was collected from the particle chamber. The material
135 obtained was stored in a desiccator containing silica gel until required for further use. The yield from spray
136 drying was ca. 35 % w/w.

137
138 For the self-assembly process, 10 mg of the spray dried formulations was accurately weighed, added to 10
139 mL of distilled water, and sonicated for 10 min to assist with the formation of SLNs. The resultant suspension
140 was then filtered using a 0.22 µm syringe filter.

141

142 2.2 Scanning electron microscopy

143 The spray dried particles were analysed by scanning electron microscopy (SEM), which was performed using
144 a field emission microscope (FEI Quanta 200F) connected to a secondary electron detector. Samples were
145 adhered to a SEM stub with carbon-coated double-sided tape, and sputter coated with gold to render them
146 conductive prior to measurement. Particle diameters were measured using the ImageJ software (National
147 Institutes of Health). At least 100 particles were measured, and the values are reported as mean ± standard
148 deviation (S.D.).

149

150 Focused ion beam (FIB) SEM was performed by mounting samples on adhesive carbon coated aluminium
151 pads and coating them with carbon in a Balzers CED 030 carbon evaporator. FIB-SEM was then undertaken
152 in a FEI Quanta 3D FEG instrument, by first sputtering the particles of interest with platinum and subsequently
153 ablating with Ga³⁺ ions.

154

155 2.3 *Transmission electron microscopy*

156 One drop of the self-assembled SLN suspension was mixed with a drop of 1 % w/v aqueous uranyl acetate
157 solution, and the resultant mixture dropped on a carbon-coated copper grid. Transmission electron
158 microscopy (TEM) was undertaken on a JEOL KEM-2100F microscope.

159

160 2.4 *Differential scanning calorimetry*

161 Thermograms were obtained on a Q2000 differential scanning calorimeter (DSC, TA Instruments). Around 2-
162 5 mg of sample was placed in a non-hermetically sealed aluminium pan (T130425, TA Instruments). The
163 samples were heated from 0 – 110 °C at 10 °C min⁻¹ (to remove any adsorbed water), followed by cooling to
164 0 °C at 10 °C min⁻¹ and reheating to 200 °C, again at 10 °C min⁻¹. All stages were performed under a 50 mL
165 min⁻¹ flow of oxygen-free nitrogen gas. The TA Universal Analysis software was used to analyse the data.

166

167 2.5 *X-Ray diffraction*

168 X-ray diffraction (XRD) patterns were collected on a Rigaku Miniflex 600 diffractometer supplied with Cu Kα
169 radiation (1.5418 Å) at 40 kV and 15 mA. Patterns were recorded over the 2θ range 3 – 40° at a speed of 5°
170 min⁻¹.

171

172 2.6 *IR spectroscopy*

173 IR spectra were obtained from 4000 to 650 cm⁻¹ on a Perkin Elmer Spectrum 100 instrument.

174

175

176 2.7 Dynamic light scattering

177 The size of the self-assembled SLNs was quantified using dynamic light scattering (DLS) on a Zetasizer Nano
178 ZS instrument (Malvern Instruments). Each formulation was dispersed in distilled water at a concentration
179 of 1 mg mL⁻¹, and a disposable polystyrene cuvette employed for sizing. The experiment was performed in
180 triplicate, with each suspension being prepared three times. To investigate the stability of the SLNs, the
181 suspension was stored and further DLS measurements collected after 6 months.

182

183 2.8 Entrapment efficiency

184 The entrapment efficiency (EE) was calculated as follows. 3 mL of the self-assembled SLNs were loaded into
185 a filter centrifuge tube (Amicon Ultra-15, 3000 MWCO, Merck Millipore) and centrifuged at 9500 rpm for 10
186 min at 25 °C, with acceleration and brake set to 9. After centrifugation, the filtrate was recovered and
187 analysed by UV spectroscopy (Cary 100 spectrophotometer, Agilent Technologies) at 240 nm (IMC) and 265
188 nm (5-FU). %EE was calculated using Equation 1:

189

$$190 \quad \%EE = \frac{W_{total\ drug} - W_{free\ drug}}{W_{total\ drug}} \times 100$$

191 Equation 1

192 $W_{total\ drug}$ represents the overall mass of drug in the formulation, $W_{free\ drug}$ is the mass of drug present in the
193 supernatant.

194

195 2.9 Drug release studies

196 5 mL of the aqueous SLN suspension was transferred into a cellulose dialysis bag (Fisher Scientific, 3500
197 MWCO, volume/cm=1.5). The latter was then placed in an autoclave bottle containing 50 mL of phosphate
198 buffered saline (PBS; pH 6.8) or fasted state simulated intestinal fluid, FaSSIF (Biorelevant) at 37 °C, and
199 stirred at 80 rpm. 2 mL aliquots were withdrawn periodically and replaced with the same volume of fresh
200 preheated media. The aliquots were filtered (0.22 µm filter) and the drug concentration quantified by UV-vis

201 spectroscopy (Cary 100 spectrophotometer, Agilent Technologies). Experiments were performed in triplicate
202 and data are presented as mean \pm S.D.

203

204 2.10 Cell culture

205 The colorectal adenocarcinoma cell line Caco-2 (ATCC HTB-37) was employed for *in vitro* studies. Cells were
206 maintained at 37 °C, under 5 % CO₂, in Dulbecco's modified Eagle's medium (DMEM-HG; Gibco)
207 supplemented with penicillin-streptomycin (1 % v/v) and L-glutamine (1 % v/v) solutions, non-essential amino
208 acid solution (1 % v/v) (all Life Technologies), and 10 % v/v heat-inactivated fetal bovine serum (Gibco)
209 (termed "complete DMEM"). Cells were passaged until required for further studies. This process involved a
210 treatment with 0.05 % trypsin-EDTA solution. The passage numbers for the viability experiments were
211 between 26 and 30.

212

213 The human dermal fibroblast (HDF) cell line was purchased from Life Technologies (lot 771555). The cells
214 were maintained at 37 °C, under a 5 % CO₂ atmosphere, in Dulbecco's modified Eagle's medium-high glucose
215 (DMEM-HG) supplemented with 10 % (v/v) heat-inactivated fetal bovine serum (Gibco), 2 mM L⁻¹ glutamine,
216 1 % v/v MEM non-essential amino acids, gentamicin solution (100 µg mL⁻¹) and amphotericin B solution (0.25
217 µg mL⁻¹) (all Life Technologies). Cells were passaged when a confluence of 70 – 80 % was reached through
218 treatment with 0.05 % trypsin-EDTA solution. The passage number for the viability experiments was between
219 20 and 25.

220

221 For viability tests, Biolite 24 well multidish clear plates (ThermoFisher) were used. The seeding density was 5
222 x 10⁴ cells mL⁻¹, and each well contained 1 mL of media. The formulations to be tested were dispersed in
223 complete DMEM (1 mg mL⁻¹), filtered through a 0.22 µm filter, and 180 µL of the resultant SLN suspension
224 was added to the wells of the plate. The cells were incubated with the dissolved formulations for 48 h. Cell
225 viability was determined using the Alamar Blue™ cell viability assay (ThermoFisher). The reagent was
226 prepared following the manufacturer's instructions, and added to the culture plates with a reagent volume

227 equal to the volume of cell culture medium present in each well. After addition, the plate was incubated for
 228 60 minutes at 37 °C and 5 % CO₂ before absorbance at 570 nm and 600 nm was read using a SpectraMax M2e
 229 spectrophotometer (Molecular Devices). The viability of the cells was calculated using the Equation 2.

230

$$231 \quad \% \text{ viability} = \frac{100 \times (A_{570, \text{treated cells}} - A_{600, \text{treated cells}})}{(A_{570, \text{untreated cells}} - A_{600, \text{untreated cells}})}$$

232

Equation 2

233 **2.11** Permeation assays

234 Caco-2 cells were grown in complete DMEM in a Falcon® 24-multiwell insert system plate (Corning) for 21
 235 days, changing the medium every 2 days. The seeding density was 3.75 x 10⁴ cells cm⁻². On the day of the
 236 assay, the Caco-2 monolayer was washed twice with transport buffer (Hanks Balanced Salt Solution
 237 supplemented with 10 mM 4-(2-hydroxyethyl)-1-piperazineethanesulfonic acid and with the pH adjusted to
 238 7.4). The cells were left to equilibrate for 30 min at 37 °C. The assay was initiated when the donor solution
 239 (containing 200 µM of the drug) was placed on the apical side of the monolayer, and samples of 250 µL were
 240 withdrawn from the basal side at different time points over 2 h. Fresh buffer was supplied at each time to
 241 maintain a constant volume. The transepithelial electrical resistance (TEER) was measured before and after
 242 the experiment to assess the integrity of the monolayer. All experiments were performed in triplicate.

243

244 The apparent permeability coefficient (P_{app}) was calculated using the Equation 3.

$$245 \quad P_{app} = \left(\frac{dQ}{dt} \right) \times \frac{1}{AC_0}$$

246

Equation 3

247

248 Where dQ/dt is the steady state flux (µmol s⁻¹) and C₀ is the initial concentration in the donor chamber (µM),
 249 A represents the effective filter area of each well (cm²).

250

251 Samples obtained from the permeation studies were subjected to a liquid-liquid extraction using ethyl
252 acetate as the organic solvent. After the addition of ethyl acetate (2 mL) to each sample, they were vortexed
253 for 2 min and then left to separate and for the organic layer to evaporate. The latter was accelerated using
254 a stream of air.

255

256 **2.12** *High performance liquid chromatography*

257 High performance liquid chromatography (HPLC) was performed on the permeation study samples using
258 previously published and validated methods (Nassim et al., 2002). The residue from liquid-liquid extraction
259 was first reconstituted in an appropriate mobile phase. The IMC mobile phase comprised 0.5 % v/v aqueous
260 orthophosphoric acid, methanol, and acetonitrile (all Fisher) at volume ratios of 40: 20: 40. For 5-FU the
261 mobile phase was acetonitrile: water (10: 90 v/v). For both analyses, a Luna C18 column (Phenomenex) was
262 utilised with an injection volume of 10 μ L. IMC experiments were undertaken at a flow rate of 2 mL min⁻¹,
263 and 5-FU chromatograms recorded at a flow rate of 1 mL min⁻¹ (Tsvetkova, 2012).

264

265 **2.13** *Stability studies*

266 The stability of the SLNs was assessed by measuring their size immediately after fabrication, and after storage
267 at room temperature for 6 months. The spray-dried microparticles were also stored under the same
268 conditions, and a fresh batch of SLNs assembled from them after 6 months. The size of the SLNs was
269 determined by DLS in each case.

270

271 **2.14** *Statistical analysis*

272 Size data obtained from DLS were analysed using a one tailed Student's t-test. The level of significance was
273 set at $p < 0.05$. Data from cell culture experiments were statistically analysed using the MiniTab17 Software.
274 The statistical significance of differences was evaluated by one-way ANOVA using Dunnett simultaneous 95%
275 CIs tests.

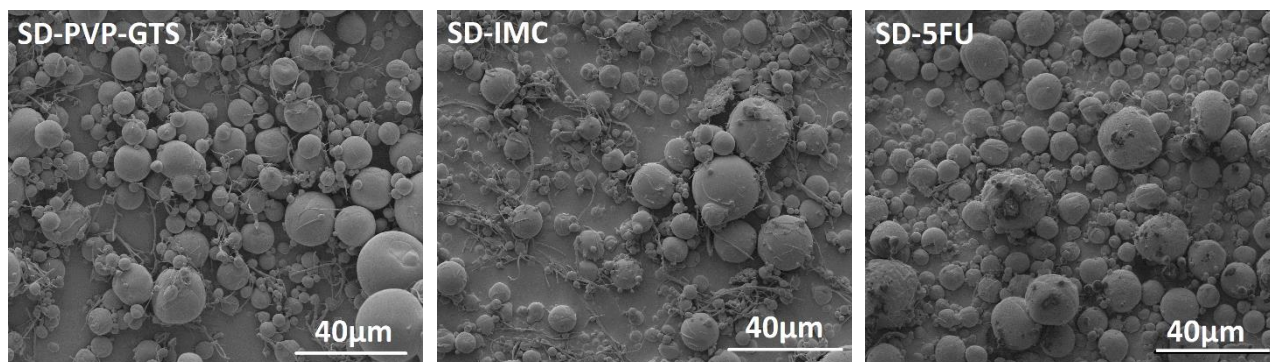
276

277 3. Results and discussion

278 3.1 Spray drying

279 The production of PVP/GTS/drug particles by spray drying was found to be facile (see Figure 2). Three
280 formulations were prepared, comprising PVP/GTS alone (SD-PVP-GTS), and PVP and GTS with IMC (SD-IMC)
281 or 5-FU (SD-5FU). All three formulations comprise spherical particles with an average size of $6.61 \pm 4.16 \mu\text{m}$
282 for SD-PVP-GTS, $7.15 \pm 4.39 \mu\text{m}$ for SD-IMC, and $5.78 \pm 4.44 \mu\text{m}$ for SD-5FU (PDIs: 0.63, 0.61 and 0.77,
283 respectively). A wide range of particle sizes have clearly formed, and in addition a few very fine fibres (due
284 to the high molecular weight of the polymer used) can be seen in all cases.

285

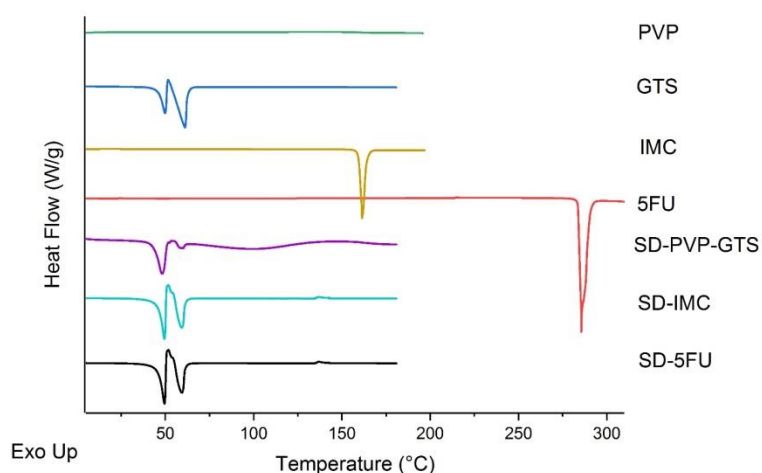


286 Figure 2: SEM images of the spray-dried formulations. SD-PVP-GTS contains PVP and GTS alone, while SD-IMC and SD-5FU also include
287 a drug (indomethacin or 5-fluorouracil respectively).

288

289 The physical form of the components in the microparticles was explored using differential scanning
290 calorimetry (DSC) and X-ray diffraction (XRD). DSC thermograms are given in Figure 3. PVP is clearly
291 amorphous: no melting peaks can be seen. The IMC data display a sharp endotherm at 161.7°C due
292 the melting of the γ -form of IMC (Dupeyrón et al., 2013). 5-FU similarly shows a sharp melting
293 endotherm at 284°C , again in agreement with the literature (Kalantarian et al., 2010). This confirms
294 both to be crystalline solids. In the case of GTS, there are two endotherms (at 49 and 60°C) and one
295 exotherm (51.2°C). The first endotherm indicates the melting of α -GTS, followed by recrystallisation
296 (exotherm) to β -GTS and then melting of the latter (second endotherm) (Singh et al., 1999a, b). GTS
297 is thus also a crystalline material. In the case of the formulations, thermograms could not be obtained

298 at temperatures above 180 °C because PVP carbonizes at 200 °C. Thus, the 5-FU melt lies outside the



299 heating range measured. The thermograms of the formulations show the same behaviour as GTS,
300 with the presence of crystalline GTS clearly present. There is no IMC melting endotherm visible in SD-
301 IMC, and thus the drug is amorphous here.

302

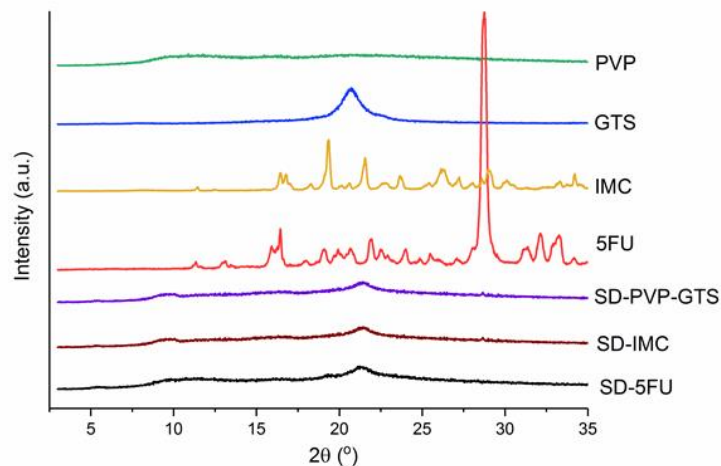
303 Figure 3: DSC thermograms showing the second heating cycle.

304

305 XRD data are shown in Figure 4. IMC is a crystalline material, with numerous distinct Bragg reflections
306 present between 10-30°, and the pattern matches that reported for the γ -form of IMC (Dupeyrón et
307 al., 2013). 5-FU also exhibits a number of Bragg reflections, confirming its crystalline nature. GTS
308 shows a Bragg reflection at 21.4°, indicating the semi crystalline nature of the material (Lutton, 1945).
309 No sharp peaks are observed in the PVP pattern, with only slight haloes at around 12 and 21°,
310 confirming it to be amorphous. Two broad halos can be observed in SD-PVP-GTS, SD-IMC and SD-5-
311 FU, one of them being a broad hump characteristic of PVP while the peak at 21.4° corresponds to
312 GTS. After spray drying, no Bragg reflections corresponding to the APIs can be seen in SD-IMC and
313 SD-5-FU. They are thus amorphously distributed in the SD particles. The spray drying process results
314 in a rapid transition from solution to solid, and thus often results in predominately amorphous

315 materials for small molecules because there is no time for crystallisation to take place (Takeuchi et
 316 al., 2005).

317



318

319 Figure 4: XRD patterns of the raw materials and formulations.

320

321 IR spectra of the raw materials and formulations can be found in Figure 5. The PVP spectrum contains
 322 two weak broad bands at $3200 - 3600\text{ cm}^{-1}$ and $2800 - 3000\text{ cm}^{-1}$, indicating O-H and C-H stretching.
 323 The O-H stretching is believed to be due to the water adsorbed by the polymer. The peak at 1660 cm^{-1}
 324 corresponds to C=O stretching. IMC displays peaks between $1580 - 1620\text{ cm}^{-1}$ from aromatic C=C
 325 stretching, C=O stretching at 1680 cm^{-1} , and bands at 1261 cm^{-1} (asymmetric aromatic O-C
 326 stretching), 1086 cm^{-1} (symmetric aromatic O-H stretching) and between $2800 - 3000\text{ cm}^{-1}$ (C-H
 327 stretching). For 5-FU, the characteristic bands are at $1429 - 1600\text{ cm}^{-1}$ (C=N and C=C ring stretching
 328 vibrations), 1720 cm^{-1} (C=O stretching), 1345 cm^{-1} (pyridine vibrations) and 2989 cm^{-1} (N-H
 329 stretching). GTS show two strong peaks at 2917 and 2850 cm^{-1} and a shoulder at 2960 cm^{-1} (C-H
 330 stretching). C=O stretching from the ester group manifests in a strong peak at 1740 cm^{-1} . Considering
 331 the formulations, the major peaks from GTS at ca. 1740 , 2917 and 2850 cm^{-1} can be observed. Other
 332 than these peaks, the spectra of the formulations are very similar to that of PVP. The characteristic
 333 carboxylate bands of IMC are shifted to lower wavenumbers and overlap with the carbonyl band of

PVP at 1660 cm^{-1} in SD-IMC. Similar observations are noted in the SD-5-FU spectrum. In both cases, this suggests the presence of interactions between the drug and polymer. This is strongly indicative that after spray drying, the composites obtained comprise homogeneous molecular dispersions of drug-in-polymer.

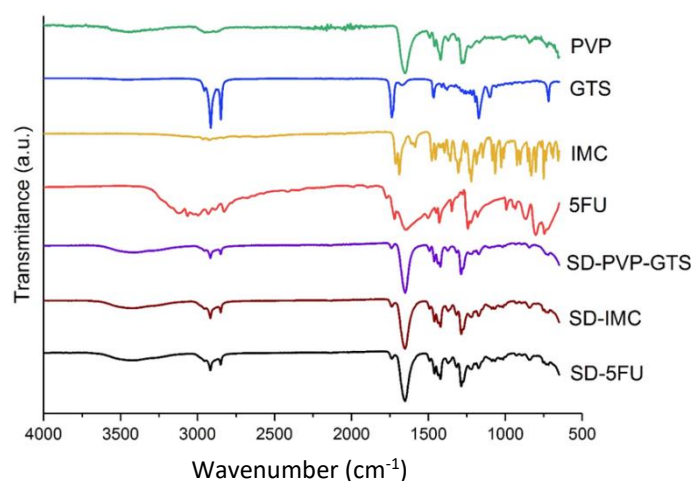


Figure 5: IR spectra.

3.2 SLN self-assembly

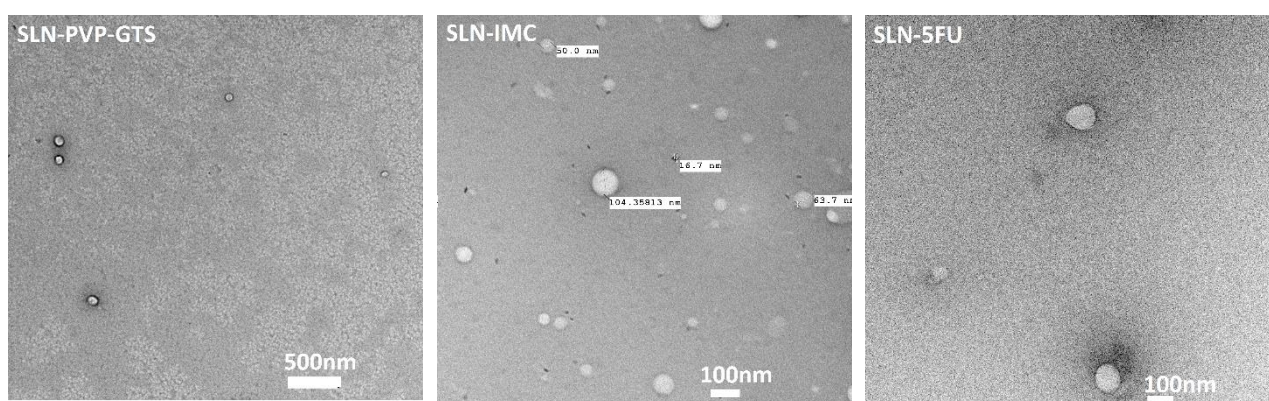
When the microparticles are added to water, smaller spherical objects of around 100 nm in size are observed in TEM images (Figure 6 and Supplementary Information, Figure S1). The products of this process are denoted SLN-PVP-GTS (generated from the spray dried PVP/GTS formulation), SLN-IMC and SLN-5FU (formed from the IMC and 5-FU-loaded formulations respectively). These are SLNs, and the images very closely resemble those previously reported in the literature (Ali et al., 2017; Kumar and Randhawa, 2015; Vieira et al., 2016; Yuan et al., 2014). From the images, the SLNs appear to be monolithic in nature, with no evidence for any core/shell morphology or phase separation. DLS (Figure 7) revealed the size of the particles to be $219 \pm 9\text{ nm}$ for SLN-IMC, $251 \pm 25\text{ nm}$ for SLN-5FU and $876 \pm 99\text{ nm}$ for SLN-PVP-GTS. The particle size is relatively homogeneous for all the drug-loaded samples, but the presence of aggregates is apparent with SLN-PVP-GTS. After filtration through a $0.22\text{ }\mu\text{m}$ membrane, the sizes are reduced to $156 \pm 3\text{ nm}$, $134 \pm 4\text{ nm}$ and $142 \pm 3\text{ nm}$ for SLN-PVP-GTS,

353 SLN-IMC and SLN-5FU, respectively. The PDIs after filtration are 0.10 ± 0.01 and 0.14 ± 0.01 for SLN-
354 IMC and SLN-5FU respectively. Any undissolved lumps and aggregates larger than $0.22 \mu\text{m}$ are
355 removed after filtration, and thus the size distributions of the SLNs become narrower.

356

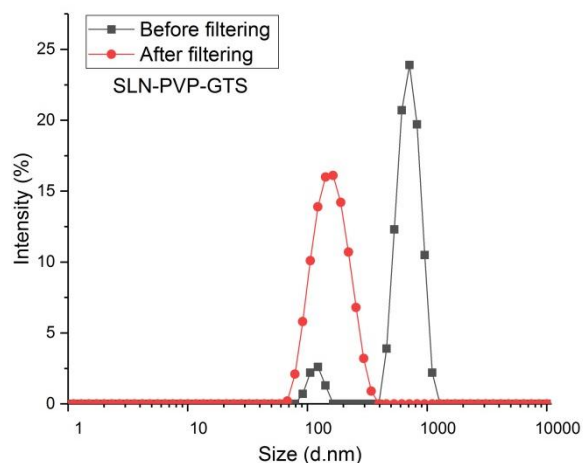
357 The formation of the SLNs can be attributed to the separation of hydrophilic and hydrophobic
358 components of the microparticles. When the PVP-based microparticles are added to water, they will
359 rapidly take up water, swell and start to dissolve. As they do so, the hydrophobic GTS and the drug
360 will tend to aggregate together, to minimise contact with the aqueous phase. This results in the
361 formation of nanoparticles comprising GTS and the drug forming as the PVP matrix is wetted,
362 disaggregates and dissolves (Yu et al., 2011b).

363

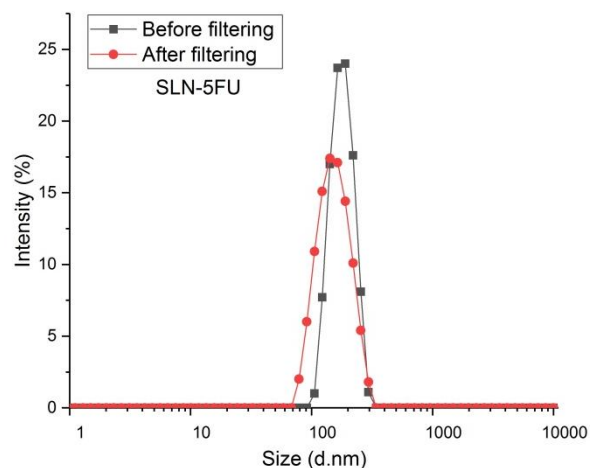


364 Figure 6: TEM images of the self-assembled SLNs. SLN-PVP-GTS are generated from the spray dried PVP/GTS formulation, while SLN-
365 IMC and SLN-5FU are formed from the indomethacin and 5-fluoruracil-loaded formulations respectively.

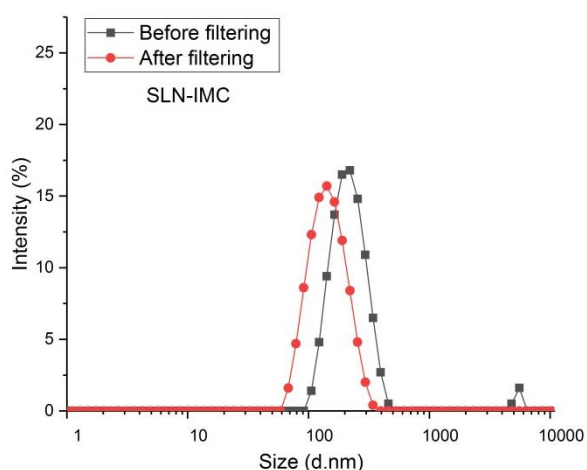
366



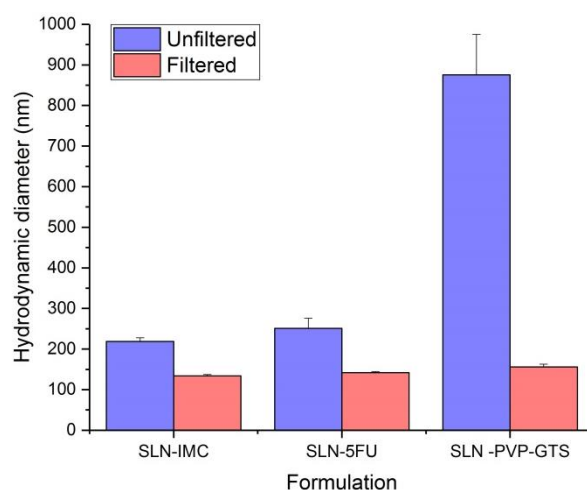
(a)



(b)



(c)



(d)

Figure 7: DLS data on the SLNs, with raw data shown for (a) SLN-PVP-GTS; (b) SLN-5FU; and, (c) SLN-IMC, together with (d) a summary of the particle sizes obtained. Data are shown both before and after filtration with a 0.22 μm syringe filter.

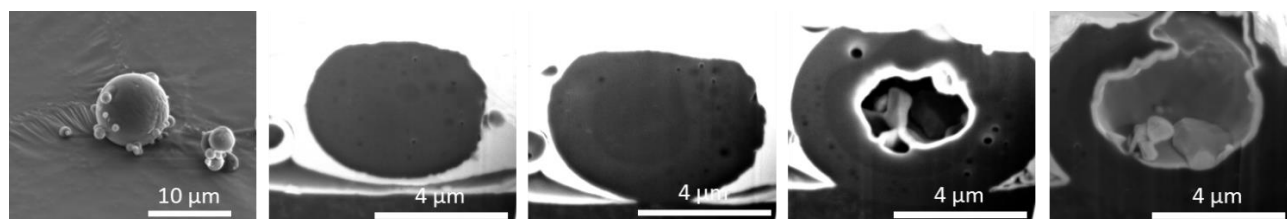
The theoretical drug loading in the formulations was 14.3 % w/w. Upon addition of SD-IMC and SD-5FU to water, the entrapment efficiency (EE) into SLNs was determined to be 86.2 ± 4.8 % and 64.9 ± 16.7 % respectively. The EE is influenced by the properties of both the lipid and the API, and thus the higher EE for SLN-IMC can be explained by the more hydrophobic nature of IMC. These EE values are similar to those reported in the literature (Du et al., 2010; Hippalgaonkar et al., 2013). The drug loading of the SLNs is 12.3 ± 0.7 % for SLN-IMC and 9.3 ± 2.4 % for SLN-5FU.

375

376 3.3 Internal structure

377 The internal structure of the spray dried SD-IMC material was explored with FIB-SEM (Figure 8). The
378 images show the particles to have a hollow structure, with some small dark objects observable in the
379 shell and some larger particles present in the core. The former are of the size of the SLNs, at ca. 100
380 – 200 nm, but they are few in number. The SLN components GTS and IMC form 43 % of the particle
381 mass, and given the relative volumes each spray dried particle should contain of the order of 10^4
382 SLNs. The FIB-SEM data thus suggest that, although some SLNs may have self-assembled during the
383 spray drying process, there is no evidence for the formation of significant numbers of nanoparticles
384 during this procedure. The images in Figure 8 indicate that there is some phase separation in the
385 spray-dried microparticles, which is consistent with the observation of semi-crystalline GTS in XRD
386 and DSC. However, the fact that large numbers of SLNs cannot be observed inside the structure
387 suggests that the situation depicted in Figure 1(d) is most likely to be correct. This is the first time
388 that such a self-assembly process has been noted from spray dried microparticles.

389



390

391 Figure 8: FIB-SEM images of SD-IMC.

392

393 3.4 Drug release

394 In this work, we sought to make formulations to treat cancers in the small intestine, ideally for oral
395 delivery. The mean pH from the small intestine to the colon varies between 6.6 and 7.5 (Evans et al.,
396 1988). Therefore, *in vitro* drug release experiments were performed using phosphate buffered saline
397 (PBS) at pH 6.8, and also fasted state simulated intestinal fluid (FASSIF). The latter is reported to
398 provide a more accurate prediction of the *in vivo* release profile of the drug than simple PBS (Vertzoni

et al., 2005). The release plots are given in Figure 9. When using PBS, it can be observed that there was a burst release of the entrapped IMC and 5-FU from the formulations in the first 7 h, and after this period slow release over 48 h. More rapid release was seen for the pure drugs. The behaviour of SLN-IMC is very similar to this in FASSIF, while SLN-5FU is much slower to release its drug cargo than in PBS. After 48 h in FASSIF, approx. 70 % of the incorporated indomethacin and 55 % of the 5-FU is released from the formulations.

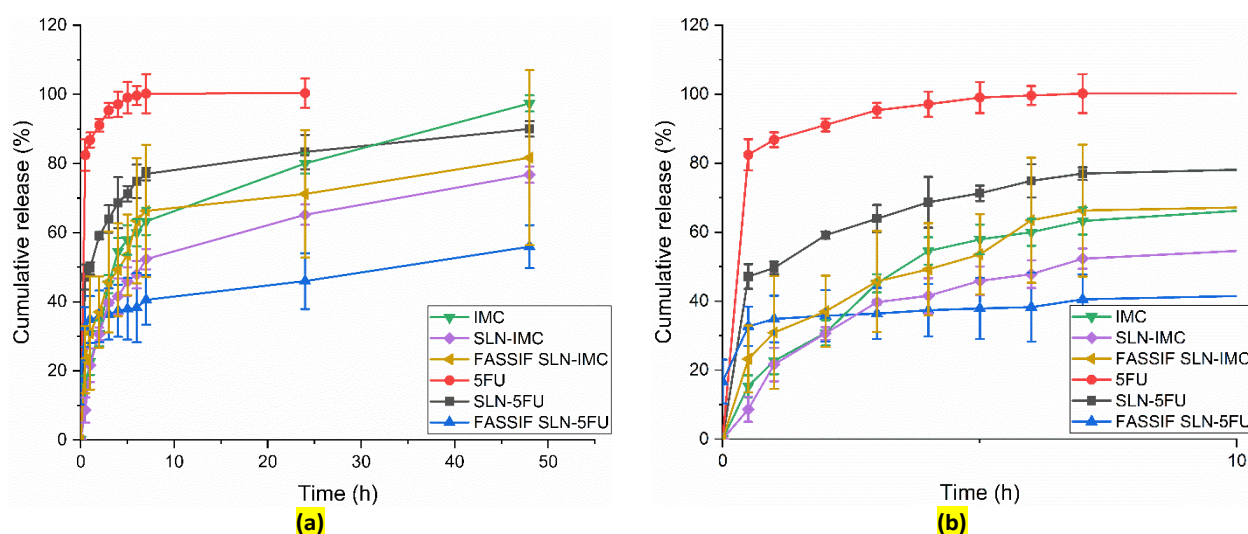


Figure 9: Drug release from the self-assembled SLNs in pH 6.8 PBS and FASSIF, showing the (a) full time-course of the experiment and (b) first 10 h (mean \pm S.D. from three independent experiments).

The transit times of the small intestine and colon are around 2.5-3 h and 30-40 h respectively (Camilleri et al., 1989; Degen and Phillips, 1996; Metcalf et al., 1987), meaning that maximum drug release would be reached while the formulations are still located in the intestinal tract after oral administration. The uptake and retention of the SLNs in tumour tissue should be augmented by the enhanced permeation and retention (EPR) effect, giving them ample time to free their drug cargo (Yassin et al., 2010). Other approaches to increase the delivery of the SLNs to cancer tissues such as targeting ligands or pH sensitive systems could also be applied (Kim et al., 2015; Tran et al., 2015). In order to ensure that the SLNs reach the colon intact, an enteric coated capsule can be used.

418 3.5 In vitro cell assays

419 3.5.1 Permeation

420 Permeation of the SLNs was explored using Caco-2 cells. The minimum inhibitory concentrations
421 (IC_{50}) were first determined and found to be 7.8 mM for IMC and 1.7 mM for 5-FU. Permeation
422 experiments were performed below these IC_{50} values, at 0.2 mM. The SLNs containing IMC did not
423 appear to permeate through the cell layer: no drug was found in the receiver compartment, and only
424 around 5 % of the initial dose was found in the donor compartment after 2 h. At the end of the
425 permeation study, the buffer in the donor compartment was discarded and the cell monolayer was
426 lysed. Analysis of the lysate showed that approximately 78 % of the IMC from SLN-IMC was present
427 in the cell monolayer. Similarly, around 62 % of the 5-FU from SLN-5FU was found in the cell
428 monolayer and approximately 12 % in the acceptor compartment. In contrast, the percentage of pure
429 IMC in the acceptor compartment was 54 %, while for 5-FU the donor compartment contained 71 %
430 of the drug content. Less than 8 % of IMC or 5-FU was found in the cell monolayer when they were
431 administered in their pure forms.

432

433 Assessment of the permeation of pure IMC resulted in a Papp value of $11.6 \times 10^6 \text{ cm s}^{-1}$, typical for
434 biopharmaceutical classification system class II (BCS II) drugs and confirming the high permeability of
435 IMC (Lee et al., 2017). In contrast, the 5-FU Papp value was $0.10 \times 10^6 \text{ cm s}^{-1}$, consistent with the
436 literature (which shows 5-FU to have poor permeability in the Caco-2 monolayer model) (Buur et al.,
437 1996). The SLNs prepared in this work thus accumulate in the cells, while IMC permeates and 5-FU
438 remains in the donor compartment. The SLNs hence have significant advantages over either drug
439 alone. If the IMC were to permeate through tumour cells and reach the systemic circulation,
440 unwanted side effects could arise; the SLNs offer an alternative to preclude this. 5-FU alone does not
441 effectively permeate, meaning that it may pass through the body without exerting a pharmacological
442 effect. The SLNs enable both IMC and 5-FU to be effectively localised in cancer cells, ideal for the
443 treatment of tumours.

444

445 Average transepithelial resistance (TEER) values were measured at the end of the permeation
446 experiment to verify the integrity of the monolayer. The average values for the control (untreated)
447 Caco-2 cell monolayer before and after the permeation experiment were $395.1 \pm 46.6 \Omega \text{ cm}^2$ and
448 $382.0 \pm 38.2 \Omega \text{ cm}^2$, respectively. The values for SLN-IMC after the experiment were $360.9 \pm 18.5 \Omega$
449 cm^2 and for SLN-5FU $368.1 \pm 6.8 \Omega \text{ cm}^2$. It is clear that the SLNs did not have any effect on the integrity
450 of the monolayer, thus demonstrating their low toxicity at the concentrations used for this
451 experiment.

452

453

454 3.5.2 Viability

455 To evaluate the ability of the formulations to kill cancerous cells, Caco-2 cells were exposed to the
456 SLNs for 48 h, using the IC_{50} of each drug. The viability values obtained were compared to the pure
457 drugs (Figure 10(a)). SLN-IMC and SLN-5FU do not show any significant differences compared to the
458 drug alone, with cell viabilities of $58.2 \pm 7.3\%$ and $53.9 \pm 7.2\%$, respectively. This indicates that the
459 SLNs are as effective in causing the death of cancerous cells as the pure drug. Similar results were
460 seen with human dermal fibroblasts (Figure 10(b)). This indicates that the SLNs are not selective in
461 their activity, as would be expected since they are not functionalised with targeting ligands. However,
462 it does appear that the 5-FU loaded SLNs are less toxic to healthy cells than the pure drug.

463

464

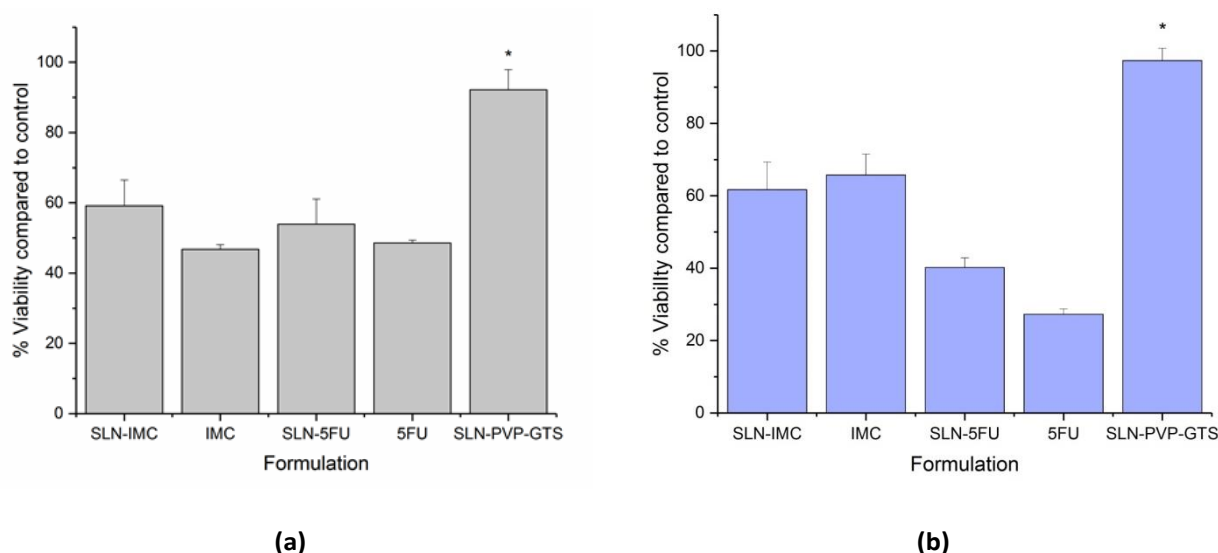


Figure 10: (a) Caco-2 and (b) HDF cell viability in the presence of pure 5-FU and IMC and the drug-loaded SLNs, determined using the Alamar Blue assay. Values represent mean \pm S.D. from three independent experiments with three replicates per experiment. Experiments were performed using the Caco-2 IC₅₀ concentration of each drug. SLNs comprising only PVP and GTS gave results significantly different to those obtained with all other formulations (* denotes $p < 0.05$).

3.6 SLN stability

One of the major issues in the use of SLNs is their long-term storage stability. The stability of SLN-IMC and SLN-5FU was thus assessed in terms of their hydrodynamic diameters after 6 months of storage at room temperature. As shown in Figure 11, while the aged suspensions of SLNs show significant changes in particle size, SLNs assembled from spray dried particles aged for 6 months have virtually the same size as those assembled immediately after spray drying. In contrast, the literature reports instability of SLN suspensions of linalool over 40 days of storage (Pereira et al., 2018) and amphotericin B after 60 days storage (Santiago et al., 2018). The poor stability of SLN suspensions arises from gelation and recrystallization of the lipid phase (Siekmann and Westesen, 1994), and by storing “proto-SLNs” in the form of spray dried particles we are able to avoid these issues.

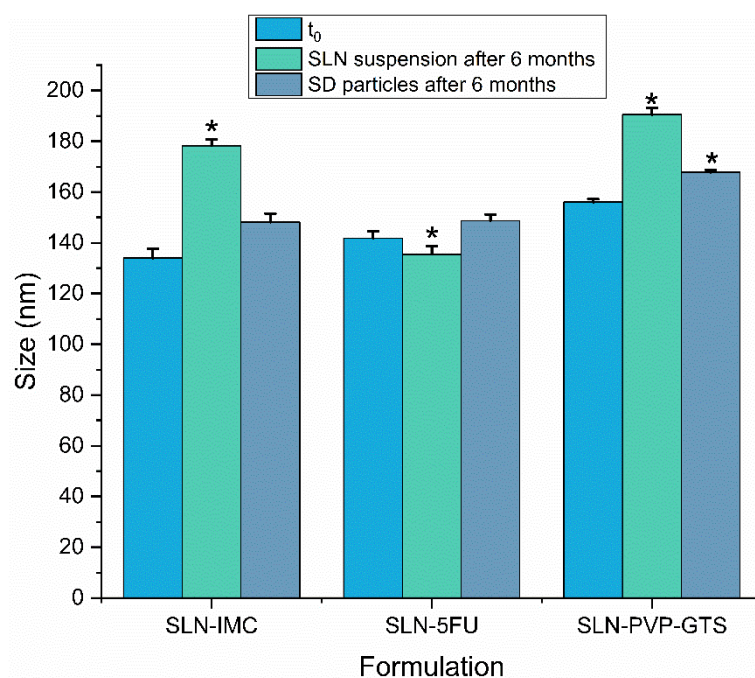


Figure 11: The results of stability studies performed for 6 months at room temperature. Data are shown from 3 independent experiments as mean \pm S.D. * denotes $p < 0.05$ with respect to those obtained at the start of the experiment (t_0).

4. Conclusions

Spray dried poly(vinylpyrrolidone) microparticles loaded with a drug and glyceryl tristearate have been shown to act as templates for the self-assembly of drug-loaded solid lipid nanoparticles (SLNs). The SLNs form upon addition of the spray dried particles to water, rather than during the spray-drying process itself. The SLNs provide a non-toxic delivery platform for both hydrophobic (indomethacin) and hydrophilic (5-fluorouracil) drugs. They have sustained release properties, and their drug cargo is seen to accumulate inside cancer cells. The SLN formulations are as efficacious as the pure drug in terms of their cytotoxicity. This work represents a novel alternative approach to the fabrication of SLNs. Because the SLNs are assembled from spray-dried microparticles on demand, the problems of instability upon storage which commonly arise with SLN formulations are obviated.

5. Conflicts of interest

There are no conflicts to declare.

498

499 6. Acknowledgements

500 BSV gratefully thanks CONACyT for the provision of a PhD studentship, and MM the Engineering and
 501 Physical Sciences Research Council (EPSRC) for PhD funding through the Centre for Doctoral Training
 502 in Advanced Therapeutics & Nanomedicines (EP/L01646X/1). GP would also like to thank the EPSRC
 503 (EP/M014649/1) and UCL (Excellence Fellowship) for financial support.

504

505 7. References

506 Ali, H., Prasad Verma, P.R., Dubey, S.K., Venkatesan, J., Seo, Y., Kim, S.-K., Singh, S.K., 2017. In vitro-in vivo and pharmacokinetic
 507 evaluation of solid lipid nanoparticles of furosemide using Gastroplus[trade mark sign]. *RSC Advances* 7, 33314-33326.
 508 Buur, A., Trier, L., Magnusson, C., Artursson, P., 1996. Permeability of 5-fluorouracil and prodrugs in Caco-2 cell monolayers.
 509 *International Journal of Pharmaceutics* 129, 223-231.
 510 Camilleri, M., Colemont, L.J., Phillips, S.F., Brown, M.L., Thomforde, G.M., Chapman, N., Zinsmeister, A.R., 1989. Human gastric
 511 emptying and colonic filling of solids characterized by a new method. *American Journal of Physiology* 257, G284-290.
 512 Chen, D.B., Yang, T.Z., Lu, W.L., Zhang, Q., 2001. In vitro and in vivo study of two types of long-circulating solid lipid nanoparticles
 513 containing paclitaxel. *Chemical and Pharmaceutical Bulletin* 49, 1444-1447.
 514 Das, S., Chaudhury, A., 2011. Recent Advances in Lipid Nanoparticle Formulations with Solid Matrix for Oral Drug Delivery. *AAPS*
 515 *PharmSciTech* 12, 62-76.
 516 Degen, L.P., Phillips, S.F., 1996. Variability of gastrointestinal transit in healthy women and men. *Gut* 39, 299-305.
 517 Démuth, B., Farkas, A., Pataki, H., Balogh, A., Szabó, B., Borbás, E., Sóti, P.L., Vigh, T., Kiserdei, É., Farkas, B., Mensch, J., Verreck, G.,
 518 Van Assche, I., Marosi, G., Nagy, Z.K., 2016. Detailed stability investigation of amorphous solid dispersions prepared by single-needle
 519 and high speed electrospinning. *International Journal of Pharmaceutics* 498, 234-244.
 520 Du, B., Yan, Y., Li, Y., Wang, S., Zhang, Z., 2010. Preparation and passive target of 5-fluorouracil solid lipid nanoparticles.
 521 *Pharmaceutical Development and Technology* 15, 346-353.
 522 Dupeyron, D., Kawakami, M., Ferreira, A.M., Cáceres-Vélez, P.R., Rieumont, J., Azevedo, R.B., Carvalho, J.C.T., 2013. Design of
 523 indomethacin-loaded nanoparticles: effect of polymer matrix and surfactant. *International Journal of Nanomedicine* 8, 3467-3477.
 524 Evans, D.F., Pye, G., Bramley, R., Clark, A.G., Dyson, T.J., Hardcastle, J.D., 1988. Measurement of gastrointestinal pH profiles in normal
 525 ambulant human subjects. *Gut* 29, 1035-1041.
 526 Farkas, B., Balogh, A., Cselko, R., Molnar, K., Farkas, A., Borbas, E., Marosi, G., Nagy, Z.K., 2019. Corona alternating current
 527 electrospinning: A combined approach for increasing the productivity of electrospinning. *International Journal of Pharmaceutics* 561,
 528 219-227.
 529 Fatnassi, M., Tourné-Péteilh, C., Cacciaguerra, T., Dieudonné, P., Devoisselle, J.-M., Alonso, B., 2010. Tuning nanophase separation
 530 and drug delivery kinetics through spray drying and self-assembly. *New Journal of Chemistry* 34, 607.
 531 Foley, P.J., Pippin, J.A., Smolock, C.J., Drebin, J.A., 2008. Growth inhibitory effects of indomethacin on human colon cancer cells are
 532 mediated, in-part, by effects on beta-catenin. *Journal of the American College of Surgeons* 207, S99.
 533 Hippalgaonkar, K., Adelli, G.R., Hippalgaonkar, K., Repka, M.A., Majumdar, S., 2013. Indomethacin-Loaded Solid Lipid Nanoparticles
 534 for Ocular Delivery: Development, Characterization, and In Vitro Evaluation. *Journal of Ocular Pharmacology and Therapeutics* 29,
 535 216-228.
 536 Hull, M.A., Gardner, S.H., Hawcroft, G., 2003. Activity of the non-steroidal anti-inflammatory drug indomethacin against colorectal
 537 cancer. *Cancer Treatment Reviews* 29, 309-320.
 538 Kalantarian, P., Najafabadi, A.R., Haririan, I., Vatanara, A., Yamini, Y., Darabi, M., Gilani, K., 2010. Preparation of 5-fluorouracil
 539 nanoparticles by supercritical antisolvents for pulmonary delivery. *International Journal of Nanomedicine* 5, 763-770.
 540 Kang, K.W., Chun, M.-K., Kim, O., Subedi, R.K., Ahn, S.-G., Yoon, J.-H., Choi, H.-K., 2010. Doxorubicin-loaded solid lipid nanoparticles
 541 to overcome multidrug resistance in cancer therapy. *Nanomedicine: Nanotechnology, Biology and Medicine* 6, 210-213.
 542 Kim, J.-H., Kim, Y., Bae, K.H., Park, T.G., Lee, J.H., Park, K., 2015. Tumor-Targeted Delivery of Paclitaxel Using Low Density Lipoprotein-
 543 Mimetic Solid Lipid Nanoparticles. *Molecular Pharmaceutics* 12, 1230-1241.
 544 Kumar, S., Randhawa, J.K., 2015. Solid lipid nanoparticles of stearic acid for the drug delivery of paliperidone. *RSC Advances* 5, 68743-
 545 68750.
 546 Lee, J.B., Zgair, A., Taha, D.A., Zang, X., Kagan, L., Kim, T.H., Kim, M.G., Yun, H.Y., Fischer, P.M., Gershkovich, P., 2017. Quantitative
 547 analysis of lab-to-lab variability in Caco-2 permeability assays. *European Journal of Pharmaceutics and Biopharmaceutics* 114, 38-42.
 548 Lee, M.K., Lim, S.J., Kim, C.K., 2007. Preparation, characterization and in vitro cytotoxicity of paclitaxel-loaded sterically stabilized
 549 solid lipid nanoparticles. *Biomaterials* 28, 2137-2146.

550 Liu, W., Wu, W.D., Selomulya, C., Chen, X.D., 2011. Facile Spray-Drying Assembly of Uniform Microencapsulates with Tunable Core–
 551 Shell Structures and Controlled Release Properties. *Langmuir* 27, 12910-12915.
 552 Lutton, E.S., 1945. The Polymorphism of Tristearin and Some of its Homologs. *Journal of the American Chemical Society* 67, 524-527.
 553 Mehnert, W., Mäder, K., 2001. Solid lipid nanoparticles: Production, characterization and applications. *Advanced Drug Delivery*
 554 *Reviews* 47, 165-196.
 555 Mehnert, W., Mäder, K., 2012. Solid lipid nanoparticles: Production, characterization and applications. *Advanced Drug Delivery*
 556 *Reviews* 64, 83-101.
 557 Metcalf, A.M., Phillips, S.F., Zinsmeister, A.R., MacCarty, R.L., Beart, R.W., Wolff, B.G., 1987. Simplified assessment of segmental
 558 colonic transit. *Gastroenterology* 92, 40-47.
 559 Mukherjee, S., Ray, S., Thakur, R.S., 2009. Solid Lipid Nanoparticles: A Modern Formulation Approach in Drug Delivery System. *Indian*
 560 *Journal of Pharmaceutical Sciences* 71, 349-358.
 561 Müller, R.H., Mäder, K., Gohla, S., 2000. Solid lipid nanoparticles (SLN) for controlled drug delivery – a review of the state of the art.
 562 *European Journal of Pharmaceutics and Biopharmaceutics* 50, 161-177.
 563 Muller, R.H., Mehnert, W., Lucks, J.S., Schwarz, C., Zur Muhlen, A., Weyhers, H., Freitas, C., Ruhl, D., 1995. Solid lipid nanoparticles
 564 (SLN) - An alternative colloidal carrier system for controlled drug delivery. *European Journal of Pharmaceutics and Biopharmaceutics*
 565 41, 62-69.
 566 Nassim, M.A., Shirazi, F.H., Cripps, C.M., Veerasingham, S., Molepo, M.J., Obrocea, M., Redmond, D., Bates, S., Fry, D., Stewart, D.J.,
 567 Goel, R., 2002. An HPLC method for the measurement of 5-fluorouracil in human plasma with a low detection limit and a high
 568 extraction yield. *International Journal of Molecular Medicine* 10, 513-516.
 569 Newman, A., 2015. *Pharmaceutical Amorphous Solid Dispersions*. Wiley.
 570 Pansare, V.J., Rawal, A., Goodwin, A., Beyerinck, R., Prud'homme, R.K., Friesen, D.T., Grass, M., Muske-Dukes, A., Vodak, D.T., 2018.
 571 Millisecond Self-Assembly of Stable Nanodispersed Drug Formulations. *Molecular Pharmaceutics* 15, 495-507.
 572 Pereira, I., Zielińska, A., Ferreira, N.R., Silva, A.M., Souto, E.B., 2018. Optimization of linalool-loaded solid lipid nanoparticles using
 573 experimental factorial design and long-term stability studies with a new centrifugal sedimentation method. *International Journal of*
 574 *Pharmaceutics* 549, 261-270.
 575 Poozesh, S., Bilgili, E., 2019. Scale-up of pharmaceutical spray drying using scale-up rules: A review. *International Journal of*
 576 *Pharmaceutics* 562, 271-292.
 577 Santiago, R.R., Gyselle de Holanda e Silva, K., Dantas dos Santos, N., Genre, J., Freitas de Oliveira Lione, V., Silva, A.L., Marcelino, H.R.,
 578 Gondim, A.D., Tabosa do Egito, E.S., 2018. Nanostructured lipid carriers containing Amphotericin B: Development, in vitro release
 579 assay, and storage stability. *Journal of Drug Delivery Science and Technology* 48, 372-382.
 580 Siekmann, B., Westesen, K., 1994. Thermoanalysis of the recrystallization process of melt-homogenized glyceride nanoparticles.
 581 *Colloids and Surfaces B: Biointerfaces* 3, 159-175.
 582 Singh, S.K., Jalali, A.F., Aldén, M., 1999a. Modulated temperature differential scanning calorimetry for examination of tristearin
 583 polymorphism: 2. Isothermal crystallization of metastable forms. *Journal of the American Oil Chemists' Society* 76, 507-510.
 584 Singh, S.K., Jalali, A.F., Aldén, M., 1999b. Modulated temperature differential scanning calorimetry for examination of tristearin
 585 polymorphism: I. Effect of operational parameters. *Journal of the American Oil Chemists' Society* 76, 499-505.
 586 Suhendi, A., Nandiyanto, A.B.D., Munir, M.M., Ogi, T., Gradon, L., Okuyama, K., 2013. Self-Assembly of Colloidal Nanoparticles Inside
 587 Charged Droplets during Spray-Drying in the Fabrication of Nanostructured Particles. *Langmuir* 29, 13152-13161.
 588 Takeuchi, H., Nagira, S., Yamamoto, H., Kawashima, Y., 2005. Solid dispersion particles of amorphous indomethacin with fine porous
 589 silica particles by using spray-drying method. *International Journal of Pharmaceutics* 293, 155-164.
 590 Tran, T.H., Ramasamy, T., Choi, J.Y., Nguyen, H.T., Pham, T.T., Jeong, J.-H., Ku, S.K., Choi, H.-G., Yong, C.S., Kim, J.O., 2015. Tumor-
 591 targeting, pH-sensitive nanoparticles for docetaxel delivery to drug-resistant cancer cells. *International Journal of Nanomedicine* 10,
 592 5249-5262.
 593 Tsvetkova, B.P.I.Z., A.; Peikov, P., 2012. High Performance Liquid Chromatographic Assay of Indomethacin and its Related Substances
 594 in Tablet Dosage Form. *International Journal of Pharmacy and Pharmaceutical Science* 4, 549-552.
 595 Valtera, J., Kalous, T., Pokorný, P., Batka, O., Bilek, M., Chvojka, J., Mikes, P., Kostakova, E.K., Zabka, P., Ornstova, J., Beran, J.,
 596 Stanishvsky, A., Lukas, D., 2019. Fabrication of dual-functional composite yarns with a nanofibrous envelope using high throughput
 597 AC needleless and collectorless electrospinning. *Scientific Reports* 9.
 598 Vass, P., Demuth, B., Farkas, A., Hirsch, E., Szabo, E., Nagy, B., Andersen, S.K., Vigh, T., Verreck, G., Csontos, I., Marosi, G., Nagy, Z.K.,
 599 2019. Continuous alternative to freeze drying: Manufacturing of cyclodextrin-based reconstitution powder from aqueous solution
 600 using scaled-up electrospinning. *Journal of Controlled Release* 298, 120-127.
 601 Vertzoni, M., Dressman, J., Butler, J., Hempenstall, J., Reppas, C., 2005. Simulation of fasting gastric conditions and its importance for
 602 the in vivo dissolution of lipophilic compounds. *European Journal of Pharmaceutics and Biopharmaceutics* 60, 413-417.
 603 Vieira, A.C., Chaves, L.L., Pinheiro, M., Ferreira, D., Sarmiento, B., Reis, S., 2016. Design and statistical modeling of mannose-decorated
 604 dapson-containing nanoparticles as a strategy of targeting intestinal M-cells. *International Journal of Nanomedicine* 11, 2601-2617.
 605 Wang, D., DuBois, R.N., 2006. Prostaglandins and cancer. *Gut* 55, 115-122.
 606 Xia, D., Shrestha, N., van de Streek, J., Mu, H., Yang, M., 2016. Spray drying of fenofibrate loaded nanostructured lipid carriers. *Asian*
 607 *Journal of Pharmaceutical Sciences* 11, 507-515.
 608 Yang, S., Zhu, J., Lu, Y., Liang, B., Yang, C., 1999. Body distribution of camptothecin solid lipid nanoparticles after oral administration.
 609 *Pharmaceutical Research* 16, 751-757.
 610 Yassin, A.E.B., Anwer, M.K., Mowafy, H.A., El-Bagory, I.M., Bayomi, M.A., Alsarra, I.A., 2010. Optimization of 5-fluorouracil solid-lipid
 611 nanoparticles: a preliminary study to treat colon cancer. *International Journal of Medical Sciences* 7, 398-408.
 612 Yu, D.-G., Williams, G.R., Yang, J.-H., Wang, X., Yang, J.-M., Li, X.-Y., 2011a. Solid lipid nanoparticles self-assembled from
 613 electrosprayed polymer-based microparticles. *Journal of Materials Chemistry* 21, 15957.

614 Yu, D.-G., Williams, G.R., Yang, J.-H., Wang, X., Yang, J.-M., Li, X.-Y., 2011b. Solid lipid nanoparticles self-assembled from
615 electrosprayed polymer-based microparticles. *J Mater Chem* 21, 15957-15961.
616 Yuan, Q., Han, J., Cong, W., Ge, Y., Ma, D., Dai, Z., Li, Y., Bi, X., 2014. Docetaxel-loaded solid lipid nanoparticles suppress breast cancer
617 cells growth with reduced myelosuppression toxicity. *International Journal of Nanomedicine* 9, 4829-4846.
618 Ziaee, A., Albadarin, A.B., Padrela, L., Femmer, T., O'Reilly, E., Walker, G., 2019. Spray drying of pharmaceuticals and
619 biopharmaceuticals: Critical parameters and experimental process optimization approaches. *European Journal of Pharmaceutical*
620 *Sciences* 127, 300-318.
621